



Observability of Inertial Rotation Axis from Light Curve Derived Relative Spin Rate Measurements

Gregory P. Badura¹ · Christopher R. Valenta¹

Accepted: 21 August 2024

© The Author(s), under exclusive licence to American Astronautical Society 2024

Abstract

Knowledge of the maneuver axis of actively controlled satellites and the rotation axes of uncontrolled satellites is critical for maintaining Space Situational Awareness (SSA) and predicting satellite motions. Estimates of the spin rate and spin-axis of rotating satellites have been shown to be retrievable via passively collected time series of satellite brightness, otherwise known as light curves. Retrieval of satellite spin state parameters from light curves is accomplished by application of a physically derived relationship, the “Epoch Method,” that explains the difference between the apparent spin rate and the inertial spin rate using the known relative motion between the observation telescope, the satellite, and the sun. There are two major challenges for retrieving the inertial spin rate from relative spin rate measurements operationally via the Epoch Method. One challenge is that satellites can have complex rotation states in the sense that they rotate about multiple axes with varying angular velocities. A second challenge is that the apparent difference between the inertial and relative spin rate is a direct function of the observer-to-solar geometry, meaning that geographical sites must be tasked optimally in order to maximize their ability to collect useful measurements for spin state retrieval. In order to overcome these challenges we derive an information metric that can both (1) explain the rotation axis that was maximally observable for a collected light curve from a geographic site, and (2) be utilized to task a diverse network of geographic sites for collecting maximally useful light curve measurements for monitoring the spin axis of an uncontrolled satellite. This is accomplished by deriving the observability of the inertial spin axis information according to the Fisher Information Matrix (FIM). We assume that the state vector that is being tracked is the inertial spin axis and that the measurement is an apparent spin rate measurement. We then derive a sensitivity matrix that utilizes the physical theory of the Epoch Method in deriving the partial derivatives of the measurement with respect to the state vector. We present several examples of how this metric can be applied towards tasking satellite networks across the continental United States for monitoring the inertial spin axis of Low Earth Orbit (LEO) and Geostationary (GEO) satellites.

Extended author information available on the last page of the article

Keywords Light curve · Spin stability · Satellite · Fisher Information · Epoch Method · Space Situational Awareness

1 Introduction

Knowledge of the rotation state of space objects is critical for many facets of Space Situational Awareness (SSA). For example, rotation state knowledge can assist with determining whether or not an object is operating in an active state because spin-stabilized satellites typically maintain a constant spin rate; consequently, a long term increase in period may indicate that a satellite is inactive [1]. Additionally, a satellite's spin rate is critical for debris tracking and remediation efforts due to the utility of this information for long-term orbit propagation and satellite breakup predictions [2–6].

An Electro-Optical (EO) means for predicting spin state is by monitoring the periodicity of brightness measurements that comprise a light curve [7, 8]. The physical theory behind these algorithms was originally developed by the astronomy community to predict the spin-axis and spin rate of comets and asteroids from passively collected telescope measurements [9, 10]. These theories have been shown to be applicable to the SSA field for both passively [7] and actively [3] collected EO light curves. In particular, the “Epoch Method” [7] that is the focus of this study has shown substantial success in determination of the spin state for satellites across Low Earth Orbit (LEO) [3, 11], Geostationary Orbit (GEO) [1, 12], and other orbital regimes [7, 13]. The “Epoch Method” essentially operates by estimating the inertial spin state (axis and rate) from relative spin rate measurements. To elaborate, there are two important definitions to consider when explaining the rotation of debris: “sidereal,” and “synodic” [3]. The synodic period is the amount of time that it takes for a spinning object to make a full revolution relative to an Earth-based telescope. The sidereal period, on the other hand, is the amount of time that it takes the object to fully rotate about its spin-axis relative to the fixed orientation of the stars [8]. In short, the synodic spin rate is the rotation rate within a relative frame while the sidereal spin rate is the rotation rate within an inertial frame.

Unfortunately, the optimization cost function that results from the “Epoch Method” derivation is highly nonlinear [3]. Studies have shown that there are often multiple candidate solutions for optimal spin axis solution when the loss function is plotted across candidate spin axis Euler angles for a single observation geometry [3, 12, 14]. These non-linearities result from physically-rooted complications such as the spin-axis ambiguity problem that is outlined in [14]. In operational terms, this non-linearity poses a major issue for correctly predicting the spin axis of a rotating satellite. One solution proposed by researchers to overcome this non-linearity is to obtain multiple observations in which the observer-target-sun geometry differs significantly in order to increase certainty in a candidate spin axis solution [3, 7]. To date, unfortunately, there has been limited research into assessing both temporal and spatial observation conditions for maximizing the confidence in a candidate spin axis. For example, in [14] the researchers show that for LEO satellite observations that the synodic and sidereal spin rates are frequently equal except for brief temporal

windows. As we will show in this paper, if the synodic and sidereal spin rates are approximately equal there is limited observability of the inertial spin axis; this can effectively render many synodic spin rate measurements of limited utility for retrieving inertial spin states, thereby wasting valuable observation time.

This paper strives to overcome such issues by proposing an inertial spin axis observability metric that is a function of satellite orbital parameters and observer location. This metric has two primary use cases that are outlined in this paper. First, the metric can be used to quantify optimal temporal windows for making measurements of a satellite with an approximately known spin axis from a fixed geographic location. Second, the metric can be used to determine the spin axes that were maximally observable for a previously collected sequence of synodic spin rate measurements. The former application has substantial utility for telescope tasking, while the latter application has utility for unmixing satellite synodic measurements when it rotates about multiple axes [1].

This paper proceeds in the following manner. In Sect. 2, we begin by outlining the theory of the “Epoch Method” in reference to our previous work in applying it to Machine Learning (ML) estimation of satellite spin properties. In Sect. 3, we outline the concept of the Fisher Information Metric (FIM) and detail the manner in which it sheds light on the observability of a state vector from measurements. In Sect. 4, we derive the FIM for a measurement of synodic spin rate for a state vector of inertial spin axis using the equations of the “Epoch Method.” In Sect. 5, we analyse retrieved FIM for insight on optimal geometries for observing a spin axis of interest. Finally, in Sect. 6 we provide realistic examples for tasking continental US satellite networks to observe LEO and GEO satellites that are spinning about defined inertial axes.

2 Theory

The Phase Angle Bisector (PAB) with respect to a Space Object (SO) body frame can be expressed via the following equation:

$$\mathbf{b}^{\mathbf{I}} = (\mathbf{o}^{\mathbf{I}} + \mathbf{s}^{\mathbf{I}}) / \|\mathbf{o}^{\mathbf{I}} + \mathbf{s}^{\mathbf{I}}\|, \quad (1)$$

where $\mathbf{o}^{\mathbf{I}}$ and $\mathbf{s}^{\mathbf{I}}$ denote the body-to-observer and body-to-sun unit vectors, respectively, and the superscript \mathbf{I} denotes that the vectors are defined in the Earth-Centered Inertial (ECI) frame. We make the note that it is only necessary that the vectors be expressed in a consistent inertial frame and that for simplicity, the ECI frame was chosen in this study. We also note that these vectors are implied to be time-dependent unit vectors but that the time (t) notation is excluded here for brevity.

The “Epoch Method” assumes that the known inertial PAB vector can be rotationally aligned into an unknown “spin-axis reference frame” that has a z -axis oriented along the SO’s spin axis and x/y -plane that is fixed in the inertial frame according to classical mechanics theorems [15]. The rotation alignment of the inertial frame vector into the spin-axis frame (denoted by superscript \mathbf{S}) is described via a rotation matrix that is dependent on Euler angles (θ, ϕ) [7]:

$$\mathbf{b}^S = \mathbf{R}(\theta, \phi) \mathbf{b}^I = \begin{pmatrix} 1 & 0 & 0 \\ 0 & \cos \theta & \sin \theta \\ 0 & -\sin \theta & \cos \theta \end{pmatrix} \begin{pmatrix} \cos \phi & \sin \phi & 0 \\ -\sin \phi & \cos \phi & 0 \\ 0 & 0 & 1 \end{pmatrix} \mathbf{b}^I \quad (2)$$

After performing the alignment into the spin-axis reference frame, the unit vector \mathbf{b}^S is then decomposed into azimuthal (Ψ) and axial (Θ) components along the frame's axes:

$$\mathbf{b}^S = [\cos \Psi \sin \Theta, \sin \Psi \sin \Theta, \cos \Theta]^T \quad (3)$$

The azimuth and axial terms of the decomposition can be written respectively as $\Psi(t, \theta, \phi)$ and $\Theta(t, \theta, \phi)$, where the dependence on both time and Euler angles is explicitly acknowledged.

The "Epoch Method" treats the azimuthal velocity of the PAB in the spin-axis frame as the primary factor accounting for the perceived difference between synodic and sidereal frequencies over time [9]. Accordingly, the expected synodic frequency (ω) at a particular time can be written as a function of the temporally constant sidereal frequency (Ω) and the spin-axis Euler angles (θ, ϕ) [7]:

$$\omega(t, \Omega, \theta, \phi) = \Omega - \frac{\partial \Psi(t, \theta, \phi)}{\partial t} = \Omega - \dot{\Psi}(t, \theta, \phi) \quad (4)$$

where the time-dependence of all terms is acknowledged in Eq. 4.

As was shown in [14], the azimuthal velocity of the PAB in the spin axis frame can be written as a function of the inertial PAB vector's direction and velocity via repeated applications of the chain rule with respect to the inertial PAB vector's coordinates:

$$\dot{\Psi}(t, \theta, \phi) = \left(\frac{-1}{ab} \right) (c \dot{b}'_x + d \dot{b}'_y + e \dot{b}'_z) = \left(\frac{-1}{ab} \right) (\boldsymbol{\sigma} \cdot \dot{\mathbf{b}}^I) \quad (5)$$

where the following simplifying scalars and vectors are defined:

$$\boldsymbol{\mu} = [\cos \phi, \sin \phi, 0]^T \quad (6)$$

$$\boldsymbol{\gamma} = [\sin \phi \sin \theta, -\cos \phi \sin \theta, \cos \theta]^T \quad (7)$$

$$a = \left(1 - (\mathbf{b}^I \cdot \boldsymbol{\gamma})^2 - (\mathbf{b}^I \cdot \boldsymbol{\mu})^2 \right)^{1/2} \quad (8)$$

$$b = \left(1 - (\mathbf{b}^I \cdot \boldsymbol{\gamma})^2 \right) \quad (9)$$

$$c = (\hat{\mathbf{x}} \cdot \boldsymbol{\mu}) \left(1 - (\mathbf{b}^I \cdot \boldsymbol{\gamma})^2 \right) + (\mathbf{b}^I \cdot \boldsymbol{\mu}) (\hat{\mathbf{x}} \cdot \boldsymbol{\gamma}) (\boldsymbol{\gamma} \cdot \mathbf{b}^I) \quad (10)$$

$$d = (\hat{\mathbf{y}} \cdot \boldsymbol{\mu}) \left(1 - (\mathbf{b}^l \cdot \boldsymbol{\gamma})^2 \right) + (\mathbf{b}^l \cdot \boldsymbol{\mu}) (\hat{\mathbf{y}} \cdot \boldsymbol{\gamma}) (\boldsymbol{\gamma} \cdot \mathbf{b}^l) \tag{11}$$

$$e = (\mathbf{b}^l \cdot \boldsymbol{\mu}) (\hat{\mathbf{z}} \cdot \boldsymbol{\gamma}) (\boldsymbol{\gamma} \cdot \mathbf{b}^l) \tag{12}$$

$$\boldsymbol{\sigma} = [c, d, e]^T \tag{13}$$

and $\hat{\mathbf{x}}$, $\hat{\mathbf{y}}$ and $\hat{\mathbf{z}}$ denote unit vectors along the x , y , and z directions, respectively.

From this equation, we can see that the observed spin rate is a nonlinear function of the PAB unit vector (\mathbf{b}^l), the unit PAB vector’s velocity ($\dot{\mathbf{b}}^l$), and the spin axis of the SO (θ, ϕ). The PAB direction and velocity time series are direct functions of the known Two-Line Element (TLE) dataset that is used to collect light curve observations of the space object [14]. Therefore, assessing the amount of inertial spin axis information that will be present in a light curve within a given temporal period can be helpful for planning sensor tasking observations for spin axis estimation. We therefore seek to determine the amount of spin axis information that is present in an observed time series as a function of observation and illumination geometry.

3 Observability and the Fisher Information Matrix

The goal of the present study is to determine the optimal time periods and geographic locations to capture relative spin rate measurements that can be utilized by algorithms (i.e. [3, 7, 14]) to infer the inertial spin axis of a tumbling space object or piece of debris. We therefore seek to determine the magnitude of information regarding the inertial spin axis that is contained within a single synodic spin rate measurement. The observability of the inertial spin axis information is captured using the Fisher Information Matrix (FIM) in this study [16]. The ($n \times n$) FIM is defined as:

$$F = E \left(\left[\frac{\partial}{\partial \mathbf{x}} \ln p(\mathbf{y}|\mathbf{x}) \right] \left[\frac{\partial}{\partial \mathbf{x}} \ln p(\mathbf{y}|\mathbf{x}) \right]^T \right) \tag{14}$$

where $\ln p(\mathbf{y}|\mathbf{x})$ is the likelihood function for a m -dimensional measurement vector (\mathbf{y}) given a n -dimensional state vector (\mathbf{x}) of interest [17]. The Fisher information matrix is a useful measure for this study’s purposes because it can be utilized to provide a scalar metric of the information about the state vector that is being tracked over time (\mathbf{x}) that is contained in an instantaneous observation (\mathbf{y}). This is due to the factor that the inverse of the FIM defines the Cramer-Rao lower bound on the estimation error covariance [16, 17].

If we make the assumption that the measurement model has the form of $\mathbf{y} = \mathbf{h}(\mathbf{x}) + \boldsymbol{\nu}$, where the measurement noise $\boldsymbol{\nu}$ is distributed as a Gaussian with zero mean and covariance \mathbf{R} , then the FIM calculation greatly simplifies [16, 17]:

$$F = \left(\frac{\partial \mathbf{h}(\mathbf{x})}{\partial \mathbf{x}} \right)^T \mathbf{R}^{-1} \left(\frac{\partial \mathbf{h}(\mathbf{x})}{\partial \mathbf{x}} \right) \quad (15)$$

The form of Eq. 15 has been shown to be useful for inferring the amount of attitude information on space objects that is present in the glints of light curves [17–19]. It is therefore applied in this study to determine the amount of information on the inertial spin axis of space debris that is present in relative spin rate measurements. The measurements are assumed to be the 1-dimensional spin rates such that $y = \omega$. The state vector of interest is assumed to be a 2-dimensional vector consisting of the inertial spin axis Euler angles, such that $\mathbf{x} = \boldsymbol{\alpha} = [\theta, \phi]$. In this study, uncertainty estimates on the relative spin rate measurements are ignored such that $v = 0$. Common practices of retrieving the relative spin rate from light curves such as the Lomb-Scargle periodogram do not allow for meaningful expression of spin rate uncertainty. This is due to factors such as temporal sampling, aliasing, and false peaks creating ambiguities in instantaneous estimates of space object spin rate [20]. Future work should focus on providing a meaningful metric of uncertainty in spin rate, but that extends beyond the scope of this theoretical study. Finally, we note that all information magnitudes that are presented in the proceeding contour plots parameterize the “information magnitude” as the square of the norm of $\partial \mathbf{h}(\mathbf{x})/\partial \mathbf{x}$. This scalar metric captures the magnitude of the only nonzero singular value of the matrix in Eq. 15, allowing for a comparison of the utility of observation sites for a given spin axis orientation [17].

4 Observability of Inertial Spin Axis from Relative Spin Rates

The goal of the following analysis is to determine the amount of spin-axis Euler angle information that is provided by a single relative spin rate measurement. To that end, the sensitivity matrix $\partial y/\partial \mathbf{x} = \partial \omega/\partial \boldsymbol{\alpha}$ is computed, where $\boldsymbol{\alpha} = [\theta, \phi]$. This 1×2 matrix is the measurement that we assume plays the role of the partial derivative $\partial h(x)/\partial \mathbf{x}$ in the FIM calculation of Eq. 15. Beginning with Eq. 4, the partial derivative $\partial \omega/\partial \boldsymbol{\alpha}$ is calculated by repeated applications of the chain rule to the equation. This can be expressed according to the following equation:

$$\frac{\partial \omega}{\partial \boldsymbol{\alpha}} = \left(\frac{\partial \dot{\Psi}}{\partial \boldsymbol{\mu}} \right) \left(\frac{\partial \boldsymbol{\mu}}{\partial \boldsymbol{\alpha}} \right) + \left(\frac{\partial \dot{\Psi}}{\partial \boldsymbol{\gamma}} \right) \left(\frac{\partial \boldsymbol{\gamma}}{\partial \boldsymbol{\alpha}} \right) \quad (16)$$

Consequently, there are four primary partial derivatives that must be derived in order to fully express the partial derivative of observed spin rate with respect to the spin-axis euler angles: $\partial \dot{\Psi}/\partial \boldsymbol{\mu}$, $\partial \dot{\Psi}/\partial \boldsymbol{\gamma}$, $\partial \boldsymbol{\mu}/\partial \boldsymbol{\alpha}$ and $\partial \boldsymbol{\gamma}/\partial \boldsymbol{\alpha}$. These are matrices of shapes (1×3) , (1×3) , (3×2) , and (3×2) , respectively.

We begin with deriving the partial derivatives of the PAB azimuth velocity with respect to the vectors $\boldsymbol{\mu}$ and $\boldsymbol{\gamma}$. By utilizing the quotient rule, these matrices can be written according to the following equations:

$$\frac{\partial \Psi}{\partial \boldsymbol{\mu}} = - \left(\frac{1}{ab} \right)^2 \left\{ \left(\frac{\partial(\boldsymbol{\sigma} \cdot \mathbf{b}^I)}{\partial \boldsymbol{\mu}} \right) (ab) - \left(\frac{\partial(ab)}{\partial \boldsymbol{\mu}} \right) (\boldsymbol{\sigma} \cdot \mathbf{b}^I) \right\} \tag{17}$$

$$\frac{\partial \Psi}{\partial \boldsymbol{\gamma}} = - \left(\frac{1}{ab} \right)^2 \left\{ \left(\frac{\partial(\boldsymbol{\sigma} \cdot \mathbf{b}^I)}{\partial \boldsymbol{\gamma}} \right) (ab) - \left(\frac{\partial(ab)}{\partial \boldsymbol{\gamma}} \right) (\boldsymbol{\sigma} \cdot \mathbf{b}^I) \right\} \tag{18}$$

We must therefore derive the partial derivatives of the scalars $(\boldsymbol{\sigma} \cdot \mathbf{b}^I)$ and (ab) with respect to the vectors $\boldsymbol{\mu}$ and $\boldsymbol{\gamma}$.

Beginning with the partial derivative of $(\boldsymbol{\sigma} \cdot \mathbf{b}^I)$ with respect to the vector $\boldsymbol{\mu}$, we obtain the following equations:

$$\begin{aligned} \frac{\partial(\boldsymbol{\sigma} \cdot \mathbf{b}^I)}{\partial \boldsymbol{\mu}} &= \dot{b}'_x \left(\hat{\mathbf{x}} \left(1 - (\boldsymbol{\gamma} \cdot \mathbf{b}^I)^2 \right) + \mathbf{b}^I (\hat{\mathbf{x}} \cdot \boldsymbol{\gamma}) (\boldsymbol{\gamma} \cdot \mathbf{b}^I) \right) + \\ &\quad \dot{b}'_y \left(\hat{\mathbf{y}} \left(1 - (\boldsymbol{\gamma} \cdot \mathbf{b}^I)^2 \right) + \mathbf{b}^I (\hat{\mathbf{y}} \cdot \boldsymbol{\gamma}) (\boldsymbol{\gamma} \cdot \mathbf{b}^I) \right) + \\ &\quad \dot{b}'_z \left(\mathbf{b}^I (\hat{\mathbf{z}} \cdot \boldsymbol{\gamma}) (\boldsymbol{\gamma} \cdot \mathbf{b}^I) \right) \end{aligned} \tag{19}$$

where we have used the vector calculus proof that $\partial(\mathbf{u} \cdot \mathbf{v})/\partial \mathbf{u} = \partial(\mathbf{u}^T \mathbf{v})/\partial \mathbf{u} = \mathbf{v}$ [21].

We next take the partial derivative of $(\boldsymbol{\sigma} \cdot \mathbf{b}^I)$ with respect to the vector $\boldsymbol{\gamma}$:

$$\begin{aligned} \frac{\partial(\boldsymbol{\sigma} \cdot \mathbf{b}^I)}{\partial \boldsymbol{\gamma}} &= \dot{b}'_x \left(-2(\hat{\mathbf{x}} \cdot \boldsymbol{\mu}) (\boldsymbol{\gamma} \cdot \mathbf{b}^I) \mathbf{b}^I + (\boldsymbol{\mu} \cdot \mathbf{b}^I) \left[\hat{\mathbf{x}} \mathbf{b}^{I^T} + \mathbf{b}^I \hat{\mathbf{x}}^T \right] \boldsymbol{\gamma} \right) + \\ &\quad \dot{b}'_y \left(-2(\hat{\mathbf{y}} \cdot \boldsymbol{\mu}) (\boldsymbol{\gamma} \cdot \mathbf{b}^I) \mathbf{b}^I + (\boldsymbol{\mu} \cdot \mathbf{b}^I) \left[\hat{\mathbf{y}} \mathbf{b}^{I^T} + \mathbf{b}^I \hat{\mathbf{y}}^T \right] \boldsymbol{\gamma} \right) + \\ &\quad \dot{b}'_z \left((\boldsymbol{\mu} \cdot \mathbf{b}^I) \left(\left[\hat{\mathbf{z}} \mathbf{b}^{I^T} + \mathbf{b}^I \hat{\mathbf{z}}^T \right] \boldsymbol{\gamma} \right) \right) \end{aligned} \tag{20}$$

where we have used the associative property of matrix multiplication, the identity of $\partial(\mathbf{v}^T \mathbf{U} \mathbf{v})/\partial \mathbf{v} = (\mathbf{U}^T + \mathbf{U}) \mathbf{v}$, and the identity of $\partial(\mathbf{u} \cdot \mathbf{v})/\partial \mathbf{u} = \partial(\mathbf{u}^T \mathbf{v})/\partial \mathbf{u} = \mathbf{v}$ [21].

We next determine the partial derivative of the scalar (ab) with respect to the vectors $\boldsymbol{\mu}$ and $\boldsymbol{\gamma}$. We begin by noting that (ab) can be written in the following expanded form:

$$\begin{aligned} ab &= (1 - 3(\boldsymbol{\gamma} \cdot \mathbf{b}^I)^2 + 3(\boldsymbol{\gamma} \cdot \mathbf{b}^I)^4 - (\boldsymbol{\gamma} \cdot \mathbf{b}^I)^6 - (\boldsymbol{\gamma} \cdot \mathbf{b}^I)^4 (\boldsymbol{\mu} \cdot \mathbf{b}^I)^2 \\ &\quad + 2(\boldsymbol{\gamma} \cdot \mathbf{b}^I)^2 (\boldsymbol{\mu} \cdot \mathbf{b}^I)^2 - (\boldsymbol{\mu} \cdot \mathbf{b}^I)^2)^{\frac{1}{2}} \end{aligned} \tag{21}$$

From this, we obtain the following partial derivative vectors:

$$\frac{\partial(ab)}{\partial \boldsymbol{\mu}} = \left(\frac{1}{2ab} \right) \left(-2(\boldsymbol{\gamma} \cdot \mathbf{b}^I)^4 (\boldsymbol{\mu} \cdot \mathbf{b}^I) + 4(\boldsymbol{\gamma} \cdot \mathbf{b}^I)^2 (\boldsymbol{\mu} \cdot \mathbf{b}^I) - 2(\boldsymbol{\mu} \cdot \mathbf{b}^I) \right) \mathbf{b}^I \tag{22}$$

Fig. 1 Information magnitude plotted on a logarithmic scale as a function of inertial spin axis (α) for 6 vectors that are perturbed from the following cardinal axes of PAB direction (\mathbf{b}^j): **a** x-axis, **b** xy-axis, **c** y-axis, **d** yz-axis, **e** z-axis, and **f** xz-axis

$$\frac{\partial(ab)}{\partial\gamma} = \left(\frac{1}{2ab}\right) (-6(\gamma \cdot \mathbf{b}^I) + 12(\gamma \cdot \mathbf{b}^I)^3 - 6(\gamma \cdot \mathbf{b}^I)^5 - 4(\gamma \cdot \mathbf{b}^I)^3(\mu \cdot \mathbf{b}^I)^2 + 4(\gamma \cdot \mathbf{b}^I)(\mu \cdot \mathbf{b}^I)^2) \mathbf{b}^I \quad (23)$$

Equations 19 and 22 can then be plugged into Eqs. 17 and 20 and 23 can be plugged into 18 to yield the necessary vectors $\partial\Psi/\partial\mu$ and $\partial\Psi/\partial\gamma$.

The remaining (3×2) matrices that must be derived are $\partial\mu/\partial\alpha$ and $\partial\gamma/\partial\alpha$. These are simple to solve for using to the derivatives of sine and cosine:

$$\frac{\partial\mu}{\partial\alpha} = \begin{bmatrix} 0 & 0 & 0 \\ -\sin\phi & \cos\phi & 0 \end{bmatrix}^T \quad (24)$$

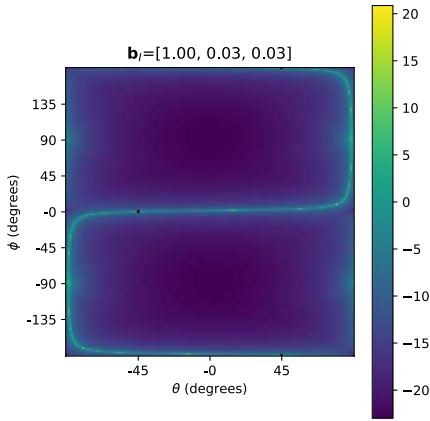
$$\frac{\partial\gamma}{\partial\alpha} = \begin{bmatrix} \sin\phi \cos\theta & -\cos\phi \cos\theta & -\sin\theta \\ \cos\phi \sin\theta & \sin\phi \sin\theta & 0 \end{bmatrix}^T \quad (25)$$

Plugging Eqs. 17, 18, 24, and 25 into Eq. 16 provides the necessary partial derivative for calculation of the FIM magnitude metric. As we will show in the proceeding sections, analysing the information magnitude as a function of the PAB direction and spin axis Euler angles provides useful insight into the optimal windows of observability for inferring the spin axis from a time series of relative spin rate measurements.

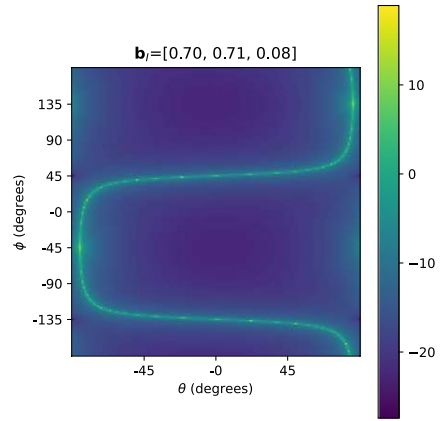
5 Effect of Phase Angle Bisector (PAB) Direction on Observability

We begin by studying the information magnitude metric that was presented in Sect. 3 as a function of the full range of possible Euler angle values over the ranges of $\theta \in [-\pi/2, \pi/2]$ and $\phi \in [-\pi, \pi]$ radians. The goal of the present Section is to understand how a given PAB directional vector (\mathbf{b}^j) influences the information magnitude as the inertial spin axis (α) of the space object varies. With this goal in mind, we consider 6 cardinal axes of the PAB direction vector and plot the information magnitude over the full range of spin axis Euler angles. The information magnitude of these six cardinal axes as a function of α is shown in Fig. 1.

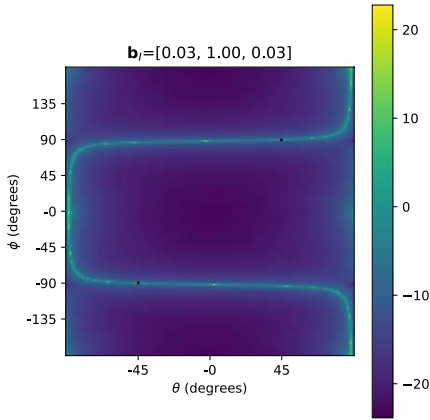
One thing that becomes immediately apparent from the information magnitude plots in Fig. 1 is that there is a unique line of maximum information for each PAB directional vector. Another thing that is apparent is that we have plotted PAB directional vectors that are moderately perturbed from the cardinal axes of interest. This is because the information magnitude goes to infinity along each line of maximal magnitude when the PAB vector is oriented along the respective cardinal axis, making it difficult to visualize the grid via contour plot means. To understand why this



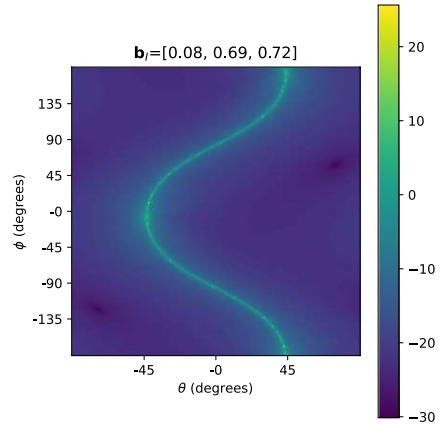
(a)



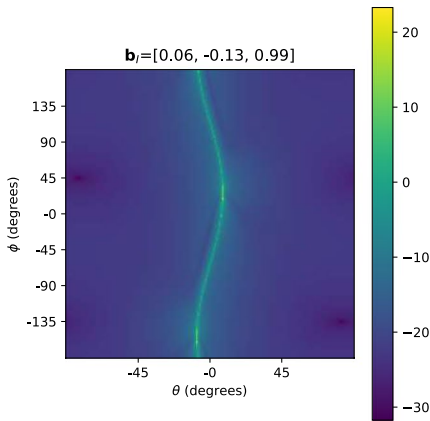
(b)



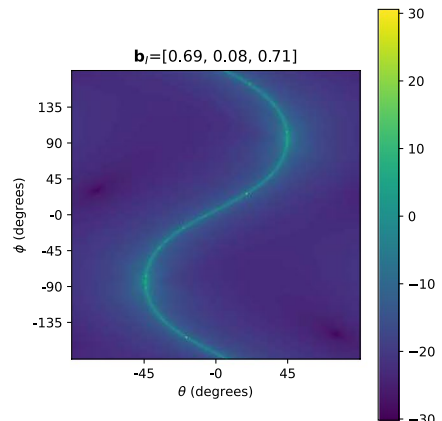
(c)



(d)



(e)



(f)

occurs, we must examine the partial derivative of the relative spin rate with respect to the spin axis that was presented in Eq. 16.

Equation 16 has the product of scalars a (Eq. 8) and b (Eq. 9) in the denominator. Therefore, as the value of either of these scalars approaches zero, the information magnitude will rapidly approach infinity. By expanding these two scalars as a function of $\boldsymbol{\alpha}$ and \mathbf{b}^I , the reason for the lines of maximum information magnitude in Fig. 1 can be readily understood in the context of PAB directions that lead to the denominator of the norm of $\partial\omega/\partial\boldsymbol{\alpha}$ approaching a value of 0:

$$a = \left(1 - (\mathbf{b}^I \cdot \boldsymbol{\gamma})^2 - (\mathbf{b}^I \cdot \boldsymbol{\mu})^2\right)^{1/2}$$

$$a = \left(1 - \left(b_x^I \sin \phi \sin \theta - b_y^I \cos \phi \sin \theta + b_z^I \cos \theta\right)^2 - \left(b_x^I \cos \phi - b_y^I \sin \phi\right)^2\right)^{1/2} \quad (26)$$

$$b = \left(1 - (\mathbf{b}^I \cdot \boldsymbol{\gamma})^2\right) = 1 - \left(b_x^I \cos \phi - b_y^I \sin \phi\right)^2 \quad (27)$$

From Eqs. 26 and 27, it is easy to observe that as the magnitudes of either $(\mathbf{b}^I \cdot \boldsymbol{\gamma})^2$ or $(\mathbf{b}^I \cdot \boldsymbol{\gamma})^2 + (\mathbf{b}^I \cdot \boldsymbol{\mu})^2$ approach 1, the denominator approaches a value of zero. The information metric magnitude consequently approaches a value of infinity.

This concept is demonstrated for a \mathbf{b}^I direction that is approximately oriented into the x -axis cardinal direction by the information magnitude contour plot in Fig. 1a. For this PAB directional vector, Eq. 27 simplifies into $b \approx 1 - (\cos \phi)^2$. Therefore, inertial spin axis observability will be maximized for all zenith angles (θ) that are oriented along the azimuth $\phi = 0^\circ$ angle of the inertial frame. Similarly, the case of \mathbf{b}^I that is perturbed from the z -axis cardinal direction produces the information magnitude contour plot of Fig. 1c. For this orientation of \mathbf{b}^I , Eq. 26 produces a value of $a \approx 1 - (\cos \theta)^2$. Consequently, it can be observed in Fig. 1c that the line of maximal information magnitude occurs for all azimuth angles (ϕ) along the $\theta = 0^\circ$ angle of the inertial frame. Interestingly, it can also be noted from Fig. 1b, d, and e that PAB vectors oriented along the xy , yz , and xz axes, respectively, produce lines of maximal information that resemble sinusoidal curves with differing phasing along the $\theta = 0^\circ$ line.

6 Optimal Geographic and Temporal Windows for Spin Axis Estimation

The previous Section provided an abstract overview of the information magnitude metric in relation to stationary cardinal directions of the PAB directional vector. In this Section, we extend those concepts towards understanding how the information metric can be leveraged in order to plan observation campaigns for satellites with time-varying PAB directional vectors. This time-varying observability metric can

ultimately be used to inform sensor tasking networks of the optimal times to observe tumbling satellites or space debris for estimation of the inertial spin axis.

6.1 Low Earth Orbit (LEO) Satellite Scenario

We first consider a scenario of a Low Earth Orbit (LEO) satellite passing over the continental United States of America (USA). A Starlink satellite (N52595) was chosen arbitrarily based on its relatively long ground trajectory over the continental USA and the appropriate solar phasing of the chosen trajectory. We note that this is an actively controlled satellite that is not tumbling, and that our choice was solely influenced by its useful trajectory properties for demonstrating our information metric on a LEO satellite. The publicly available Two Line Element (TLE) data for the chosen LEO satellite is given in Listing 1, as obtained from Celestrak [22]. The track of the sub-satellite Latitude and Longitude coordinates are plotted along the red trajectory in Fig. 2a. This pass occurred over the time

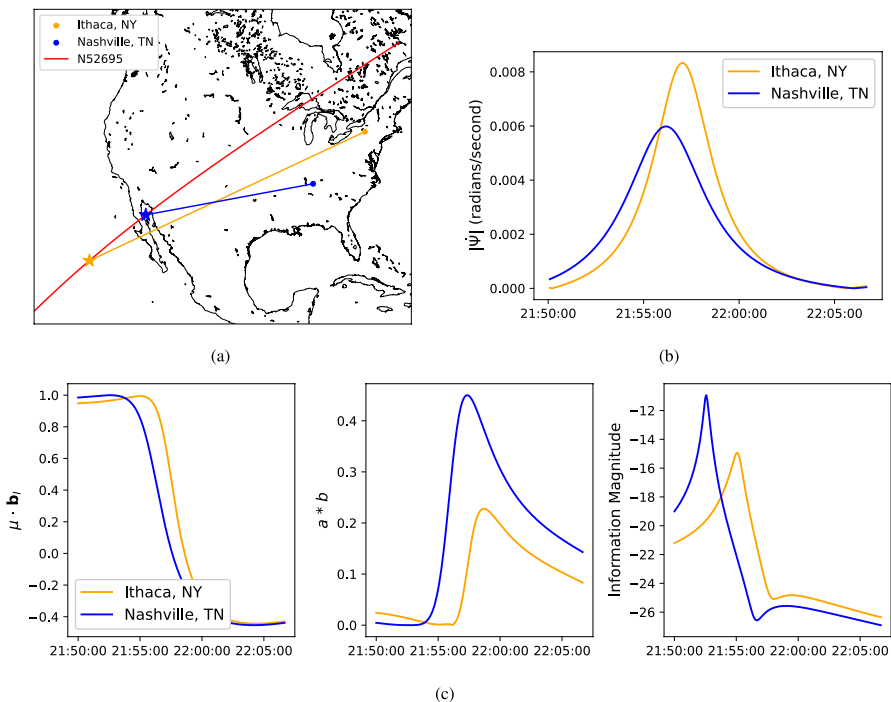


Fig. 2 A scenario of Starlink 4041 (NORAD ID 52695, TLE in Listing 1) passing over the United States and being observed from theoretical telescope locations in Ithaca, New York and Nashville, Tennessee. The window of this pass occurred on September 28, 2023 from 21:50:00 to 22:05:00 UTC. **a** shows the geometry of the pass and the collection lines of sight for a single moment of the pass. **b** show the velocity of the PAB azimuthal velocity over the course of the pass. **c** shows components that are used in the information magnitude calculation, demonstrating the brief spike in information magnitude at each site over the pass being due to the factor ab

period spanning from 21:50:00 to 22:05:00 Universal Time Coordinated (UTC). We simulated an observation from a continental USA for an uncontrolled satellite occupying this orbital slot and spinning about an axis of ($\theta = 60^\circ$, $\phi = 30^\circ$).

Listing 1: Two Line Element (TLE) information that was used to generate a satellite trajectory for Starlink 4041 (NORAD ID 52695) passing over the United States in Figure 2.

```
1 52695U 22053AR 23270.51509479 -.00004302 00000-0 -25248-3 0 9998
2 52695 53.2166 203.0248 0001320 84.9874 275.1269 15.08826539 75693
```

As was discussed in our previous work on retrieval of inertial spin axis from relative spin rate measurements [14], capturing relative spin rate measurements (ω) at non-optimal observation geometries leads to the relative spin rate being approximately equal to the inertial spin rate (Ω). To demonstrate this phenomenon, we use the ephemeris- and TLE-derived observation and solar geometry over the time of the simulation to generate the magnitude of the PAB azimuthal velocity ($|\dot{\Psi}|$) as observed from two observation sites: Ithaca, New York and Nashville, Tennessee. The time series of the magnitude of the PAB azimuthal velocity as observed from these two different sites is shown in Fig. 2b. Additionally, the sub-satellite Latitude and Longitude for the moment at which the value of $|\dot{\Psi}|$ is maximized for each site is shown by a color-coded star along the satellite ground trajectory in Fig. 2a. From Fig. 2b, it can be observed that the value of $|\dot{\Psi}|$ at these two geographically distant sites follows a similar pattern at which the value of $|\dot{\Psi}|$ rapidly rises and falls to zero. Because it is only over these time periods that the relative spin rate (ω) substantially differs from the inertial spin rate (Ω), it is only during these time periods for which $|\dot{\Psi}|$ is greater than zero that the spin axis Euler angle is observable according to Eq. 16.

This insight can be proven by analyzing the information magnitude metric that was derived in Sect. 4. The value of the scalar dot product of the PAB direction with the $\boldsymbol{\mu}$ vector ($\mathbf{b}^I \cdot \boldsymbol{\mu}$) is shown in Fig. 2c. It can be observed that there is a brief moment for which the $\boldsymbol{\mu}$ vector is parallel to the PAB directional vector, at which time the $\mathbf{b}^I \cdot \boldsymbol{\mu}$ is approximately equal to 1. This leads to the the denominator of the PAB information metric (ab) approaching a value of zero as shown in Fig. 2c, and the information magnitude simultaneously spiking to a maximum as shown in Fig. 2e. Interestingly, the information magnitude spike in Fig. 2c occurs prior to the maximization of the magnitude of the PAB azimuthal velocity in Fig. 2b. This suggests that the time rate of change of $|\dot{\Psi}|$ drives the observability of inertial spin axis from relative spin rate measurements.

Analyzing the information magnitude as the LEO satellite crosses over the full span of the continental USA provides greater insight into why these cities were chosen in our example. In Fig. 3, we show a heatmap of the information magnitude when plotted over the USA for several timesteps of the scenario that was outlined in Fig. 2. This heatmap reveals that the peak of the information magnitude moves like a spotlight over the Eastern continental USA for the case of LEO objects passing overhead. This example highlights that when attempting to retrieve the inertial spin axis of LEO space debris and tumbling space objects, having a diverse satellite

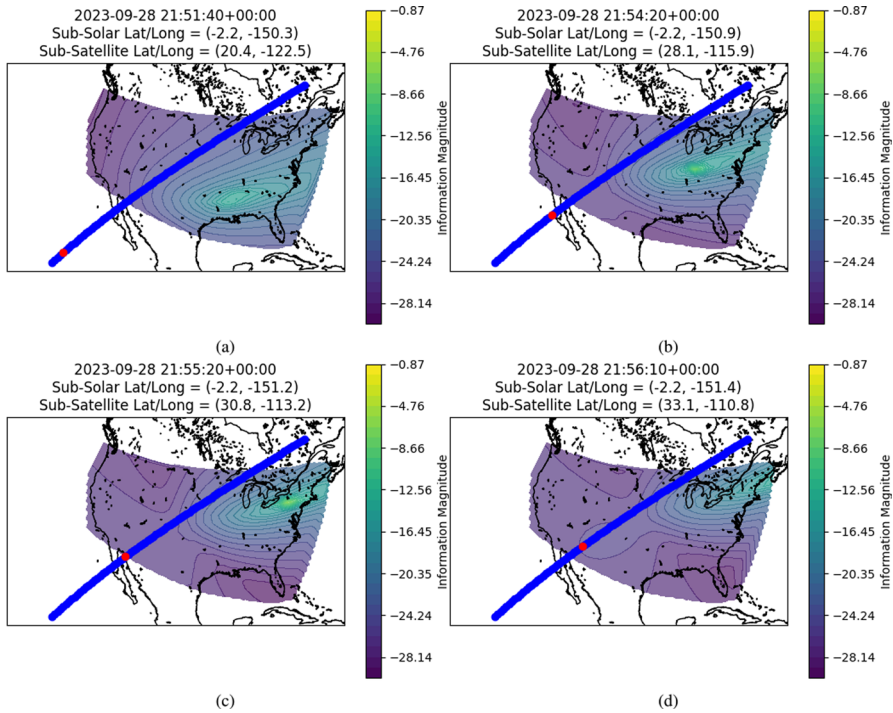


Fig. 3 Heat map showing the information magnitude across the continental USA for a pass of Starlink 4041 (N52695). The trajectory over the time period on September 28, 2023 from 21:50:00 to 22:05:00 UTC is shown in blue and the current trajectory point is shown in red for each snapshot. Note that the log of the information magnitude is plotted to enhance visualization

network is critical due to the relatively short time spans for which the inertial spin axis will be observable by any individual Latitude and Longitude coordinate.

6.2 Geostationary Orbit (GEO) Satellite Scenario

The scenario in the previous sub-section presented an example of a LEO satellite crossing the USA. It is also of interest to infer what a GEO satellite’s spin axis observability would look like from the perspective of a continental USA telescope network. Therefore, the GEO satellite Sirius XM-8 (SXM-8) (N48838) was utilized in a different simulation scenario. We once again note that this is an active satellite that was chosen solely based on its preferential geostationary slot for light curve observations from the continental USA. The publicly available TLE data for the SXM-8 GEO satellite is given in Listing 2, as obtained from Celestrak [22]. We simulated observations of an uncontrolled satellite occupying the SXM-8’s orbital slot and spinning about an axis of ($\theta = 85^\circ$, $\phi = 90^\circ$) over a time period spanning from 04:00:00 to 13:00:00+00:00 UTC on September 28, 2023. We note that the

local satellite altitude and local solar altitude were not considered, as the focus was only on the PAB's velocity.

Listing 2: Two Line Element (TLE) information that was used to generate a satellite trajectory for GEO satellite SXM-8 (NORAD ID 48838) in its stationary orbit over South America.

```
1 48838U 21049A 23277.06235826 -.00000214 00000-0 00000+0 0 9997
2 48838 0.0212 243.3874 0003188 132.9081 293.4477 1.00273075 8721
```

The magnitude of the change in the apparent spin rate, $|\dot{\Psi}|$, for the uncontrolled GEO satellite when observed from two sites on opposite coasts of the USA (Orlando, FL and Los Angeles, CA) is shown in Fig. 4a. It is apparent that the relative spin rate (ω) differs from the inertial spin rate (Ω) for far greater periods of time than in the case of LEO satellites, with the window of spin axis observability potentially lasting for over 10 h. However, it can also be seen that the magnitude of the change in the apparent spin rate is smaller than that of the LEO satellite and therefore that the precision of the spin rate estimation techniques must be higher if applied to GEO light curve observations.

The scalar dot product of the time-varying PAB directional vector with the μ vector for our simulated spin axis is shown in Fig. 4b. It can be seen that despite the increased amount of time for which the GEO satellite's apparent spin rate differs from the inertial spin rate, there is still only a brief window for which the μ vector is

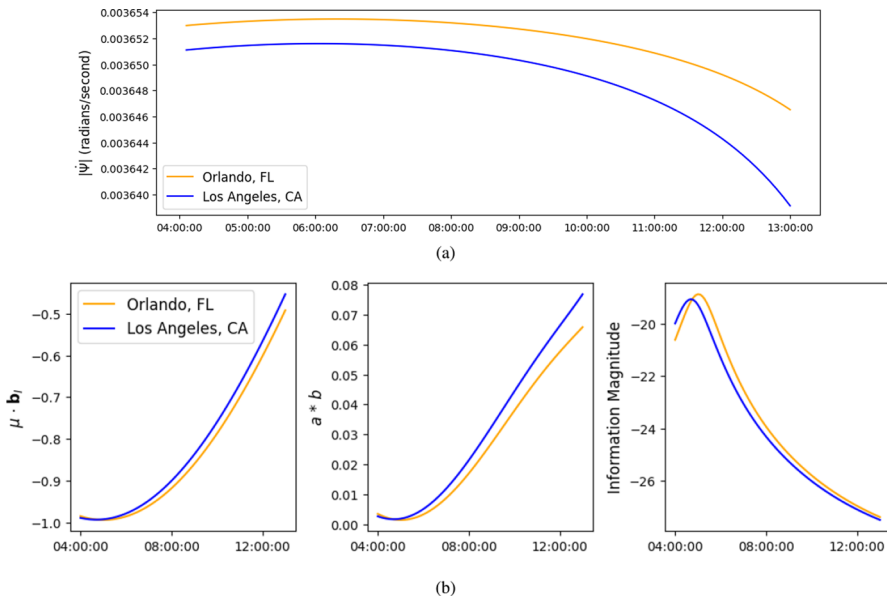


Fig. 4 A scenario of SXM-8 (NORAD ID 48838, TLE in Listing 1) being observed from two coastal sites in the USA. The window of this pass occurred on September 28, 2023 from 04:00:00 to 13:00:00+00:00 UTC. **a** shows the PAB azimuthal velocity over the course of the pass. **b** shows components that are used in the information magnitude calculation, demonstrating that there is a long duration (i.e. hour long) peak in observability

approximately parallel to the PAB directional vector. This consequently leads to the denominator of the PAB information metric (ab) approaching the optimal observability value of zero for only a brief moment of time. In terms of spin axis observability, this translates into a relatively sharp spike of maximum information magnitude as seen in the plot in the righthand side of Fig. 4b. However, the peak-to-tail information magnitude ratio is relatively smaller for the case of the GEO satellite than in the case of the LEO satellite. Additionally, the tail falls off much more slowly for our simulated GEO scenario than in our simulated LEO scenario. We acknowledge that these results are drawn from only a single GEO satellite being observed from two observation sites. However, this insight suggests that estimating the spin axis of GEO satellites is less sensitive to the time of observation than the case of estimating the spin axis of LEO satellites. This is likely due to the fact that all PAB azimuthal velocity is caused by the (relatively) slowly changing direction of the sun relative to the satellite, as the satellite-to-observer line of sight is fixed with respect to time for a GEO satellite.

To understand this concept further, we plot the information magnitude of the GEO scenario as a contour map across the continental USA for four selected times of observation in Fig. 5. If the LEO information magnitude contour map was characterized as a spotlight, the GEO information magnitude contour map should be characterized as a floodlight. It can be observed that the peak maximum

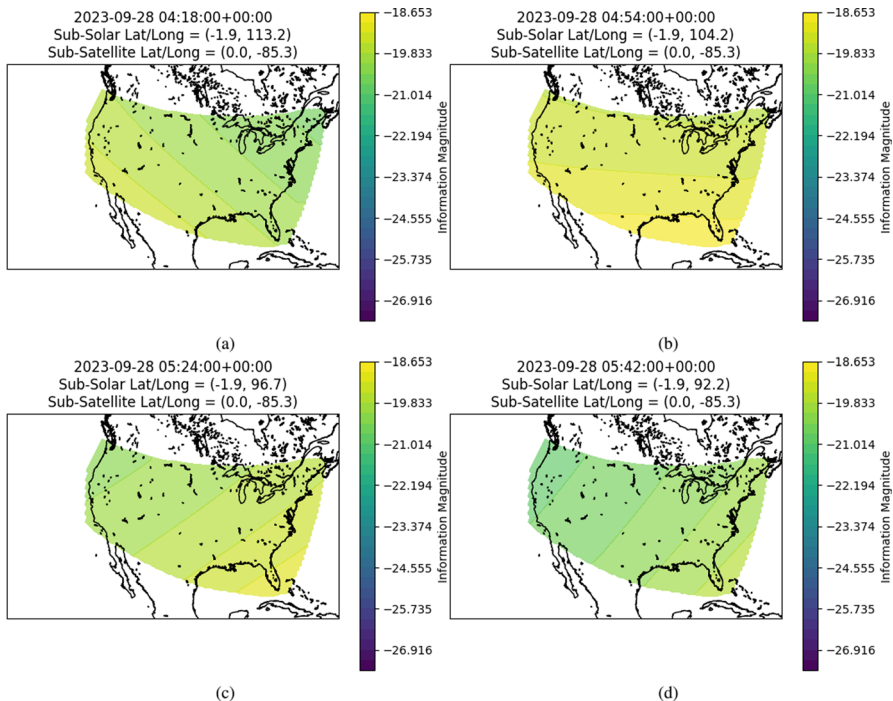


Fig. 5 Heat map showing the information magnitude across the continental USA for a pass of SXM-8 (N48838)

information magnitude spans a broad swath of the continental USA for a vast majority of the observation window. At the start of the simulation (4:18:00 UTC), the peak information magnitude is concentrated on the southwestern coast of the USA. At the middle of the observation window (4:54:00 UTC), nearly the entire southern USA spanning both coasts has a viable opportunity for performing spin axis estimation. At the end of the observation window (5:24:00 UTC), the southeastern USA has optimal observing conditions for performing spin axis estimation. We believe that the insights gained from these types of simulations can drive telescope networks to intelligently task their sensors for estimating the spin axis of both orbital debris and uncontrolled satellites in the LEO and GEO regimes.

7 Conclusion

Knowledge of the spin axis of satellites is critical for tasks such as orbital propagation, breakup modeling, and anomaly detection. In this paper, we analyse the "Epoch Method" that is used in the astronomy and SSA communities for the retrieval of inertial spin axis from apparent spin rate measurements. While the "Epoch Method" has seen success in the SSA field for predicting the spin axis of satellites [3, 7, 8, 12, 14], it has well documented challenges for reliably retrieving a global optimum Euler axis solution.

One challenge is that satellites can have complex rotation states about multiple axes. The "Epoch Method" has been well-documented to generate multiple local minima candidate solutions across the search space of potential Euler angle solutions [3, 12, 14]. To overcome this challenge, researchers have suggested that multiple follow on campaigns be performed to improve the global optimum solution [7]. In spite of this recommendation, there are challenges with tasking telescope networks to achieve maximum observability of a desired spin axis. In other words, the second challenge of deploying the "Epoch method" operationally is that apparent difference between the inertial and relative spin rate as predicted by the method is a direct function of the observer-to-solar geometry. This means telescopes that are fixed at geographical sites must be tasked optimally in order to maximize their ability to collect useful measurements for inertial spin axis retrieval.

In order to overcome these challenges, we have generated an observability metric that has applications in telescope network tasking and spin axis unmixing. We derived the observability of the inertial spin axis information according to the Fisher Information Matrix (FIM) from a time sequence of synodic (i.e. relative) spin rate measurements collected by a passively observing telescope. In this paper, we also presented several practical examples of how this metric can be applied towards tasking satellite networks across the continental United States for monitoring the inertial spin axis of Low Earth Orbit (LEO) and Geostationary (GEO) satellites. We believe that this metric will have substantial utility in operationally planning campaigns to track the spin axis of debris and uncooperative satellites across time and geographic location.

References

1. Abercrombie, M.D., Calef, B., Naderi, S.: Light curve analysis of deep space objects in complex rotation states. In: *Advanced Maui Optical and Space Surveillance Technologies Conference (AMOS)* (2021)
2. Schildknecht, T.: Optical surveys for space debris. *Astron. Astrophys. Rev.* **14**, 41–111 (2007)
3. Zhao, S., Steindorfer, M., Kirchner, G., Zheng, Y., Koidl, F., Wang, P., Shang, W., Zhang, J., Li, T.: Attitude analysis of space debris using SLR and light curve data measured with single-photon detector. *Adv. Space Res.* **65**(5), 1518–1527 (2020)
4. Benson, C., Scheeres, D., Moskovitz, N.: Light curves of retired geosynchronous satellites. In: Flohrer, T., Schmitz, F. (eds). *Proceedings 7th European Conference on Space Debris*, Darmstadt, Germany, 18–21 April 2017. ESA Space Debris Office (2017)
5. Benson, C.J., Scheeres, D.J., Ryan, W.H., Ryan, E.V.: Cyclic complex spin state evolution of defunct geo satellites. In: *Proceedings of the advanced Maui optical and space surveillance technologies conference. Maui Economic Development Board Kihei, HI* (2018)
6. Benson, C.J., Scheeres, D.J., Ryan, W.H., Ryan, E.V., Moskovitz, N.A.: Goes spin state diversity and the implications for geo debris mitigation. *Acta Astronautica* **167**, 212–221 (2020)
7. Hall, D., Africano, J., Archambeault, D., Birge, B., Witte, D., Kervin, P.: Amos observations of nasa's image satellite. In: *The 2006 AMOS Technical Conference Proceedings*, pp. 10–14 (2006)
8. Hall, D., Kervin, P.: Optical characterization of deep-space object rotation states. In: *The Advanced Maui Optical and Space Surveillance Technologies (AMOS) Conference* (2014)
9. Magnusson, P., Barucci, M.A., Drummond, J.D., Lumme, K., Ostro, S.J., Surdej, J., Taylor, R.C., Zappala, V.: Determination of pole orientations and shapes of asteroids. In: Binzel, R.P., Gehrels, T., Shapley Matthews, M. (eds.) *Asteroids II*. University of Arizona Press, Tucson, pp. 66–97 (1989)
10. Magnusson, Per: Distribution of spin axes and senses of rotation for 20 large asteroids. *Icarus* **68**(1), 1–39 (1986)
11. Vananti, A., Guthruf, D., Lu, Y., Schildknecht, T.: Estimation of reflective properties from light curves of a H2A rocket body. In: Flohrer, T., Lemmens, S., Schmitz, F. (eds.) *Proceedings 8th European Conference on Space Debris (virtual)*, Darmstadt, Germany, 20–23 April 2021. ESA Space Debris Office (2021)
12. Song, C., Lin, H.-Y., Zhao, C.-Y.: Analysis of Envisat's rotation state using epoch method. *Adv. Space Res.* **66**(11), 2681–2688 (2020)
13. Kucharski, D., Kirchner, G., Koidl, F., Fan, C., Carman, R., Moore, C., Dmytrotsa, A., Ploner, M., Bianco, G., Medvedskij, M., et al.: Attitude and spin period of space debris envisat measured by satellite laser ranging. *IEEE Trans. Geosci. Remote Sens.* **52**(12), 7651–7657 (2014)
14. Badura, G.P., Valenta, Christopher R.: Physics-guided machine learning for satellite spin property estimation from light curves. In: *Proceedings of the Advanced Maui Optical and Space Surveillance (AMOS) Technologies Conference* (2023)
15. Goldstein, H., Poole, C., Safko, J.: *Classical mechanics*. Addison-Wesley, Reading (2001)
16. Crassidis, J.L., Junkins, J.L.: *Optimal Estimation of Dynamic Systems*. Chapman and Hall/CRC, Boca Raton (2004)
17. Hinks, J.C., Linares, R., Crassidis, J.L.: Attitude observability from light curve measurements. In: *AIAA Guidance, Navigation, and Control (GNC) Conference*, p. 5005 (2013)
18. Dianetti, A.D., Crassidis, J.L.: Space object material determination from polarized light curves. In: *AIAA Scitech 2019 Forum*, p. 0377 (2019)
19. Dianetti, A.D., Crassidis, J.L.: Space object attitude determination from multispectral light curves. In: *AIAA Scitech 2020 Forum*, p. 1098 (2020)
20. VanderPlas, J.T.: Understanding the lomb-scargle periodogram. *Astrophys. J. Suppl. Ser.* **236**(1), 16 (2018)
21. Petersen, K.B., Pedersen, M.S. et al. *The Matrix Cookbook*. Technical University of Denmark (2008)
22. Vallado, D., Crawford, P., Hujsak, R., Kelso, T.S.: Revisiting spacetrack report #3. In *AIAA/AAS Astrodynamics Specialist Conference and Exhibit*, p. 6753 (2006)

Publisher's Note Springer Nature remains neutral with regard to jurisdictional claims in published maps and institutional affiliations.

Springer Nature or its licensor (e.g. a society or other partner) holds exclusive rights to this article under a publishing agreement with the author(s) or other rightsholder(s); author self-archiving of the accepted

manuscript version of this article is solely governed by the terms of such publishing agreement and applicable law.

Authors and Affiliations

Gregory P. Badura¹  · **Christopher R. Valenta¹**

✉ Gregory P. Badura
Gregory.Badura@gtri.gatech.edu

¹ Georgia Tech Research Institute (GTRI) Electro-Optical Systems Laboratory (EOSL), Atlanta, USA